Science Arts & Métiers (SAM)

is an open access repository that collects the work of Arts et Métiers Institute of Technology researchers and makes it freely available over the web where possible.

To cite this version :

Theoretical analysis of self-similar crack propagation along viscoelastic and elasto–viscoplastic interface in a double cantilever beam test

J. P. Marquez Costa · J. Jumel

Abstract As well as most polymer materials, adhesives generally exhibit significant viscous behaviour over a wide temperature range. However, strain rate sensitivity, relaxation or creep phenomena are rarely explicitly considered when crack propagation phenomena along adhesively bonded joints are involved. In the present contribution, a detailed analysis of crack propagation along viscoelastic and elasto–viscoplastic interface in a double cantilever beam (DCB) test is proposed. The Nishihara Model is used for modelling the interface separation mechanical response. Assuming self-similar crack propagation regime, a Eulerian representation can be used to simplify the resolution of the constitutive equations which control the stress/strain distribution along the fracture process zone (FPZ) combined with a finite difference resolution technique to evaluate adhesive strain/stress evolution along the bondline. Parametric analysis is then proposed to evaluate the relation between crack propagation conditions and the interface rate-dependent behaviour.

J. P. Marquez Costa · J. Jumel (✉)
Institut de Recherche Dupuy de Lôme, UMR CNRS 6027), Brest, France
e-mail: julien.jumel@ensta-bretagne.fr

Present Address:
J. P. Marquez Costa
PIMM Laboratory, Procédés et Ingénierie en Mécanique Et Matériaux, CNRS-UMR 8006, ENSAM, CNRS, CNAM, Paris, France

1 Introduction

Adhesive bonding is now widely used to produce strong and durable structural assembly for demanding applications such as transportation, construction, electronics, etc. However, due to the polymeric nature of the adhesive, the durability of bonded joints in a harsh environment is limited (Majda and Skrodzewicz 2009; Barla et al. 2012; Yu et al. 2020; Fahimifar et al. 2015; Holmes et al. 2006). Indeed, elevated temperatures as well as exposure to solvents such as water are likely to accelerate creep phenomena which may lead to delayed failure. Such phenomena are dangerous since it is difficult to monitor the joint degradation in situ and because evaluation of time to failure is still unreliable (European Cooperation for Space Standardization (ECSS) 2011). Indeed, ageing mechanisms are numerous and complex so that physically based models are difficult to implement especially when couplings are involved. Then, in industrial contexts and for design purposes, standardized procedures are preferred to evaluate the time to failure as a function of ageing conditions and loading conditions. Time/temperature equivalence and accelerated ageing procedures are also suggested to evaluate long time performances of bonded assemblies. However, such

protocols remain unreliable since the testing conditions cannot reproduce the exact mechanisms involved in the joint degradation so that safety margin should be introduced. Alternatively, they may lead to significant oversizing of the joint. To achieve more reliable design of bonded assembly, damage tolerance could be used rather than safe life approach. The assembly is designed so that the ultimate failure is due to the stable onset and propagation of a cohesive decohesion along the bonded layer prior to an unstable crack propagation occurs for a known critical crack length value. Nevertheless, for this method to be applicable, the crack growth kinetic must be accurately predicted. Again, master curves could be experimentally obtained using standard protocol such as a wedge test for stationary loading conditions (Budzik et al. 2009). The slow crack growth rate is generally reported as a function of the instantaneous strain energy release rate (SERR) despite this quantity is theoretically not applicable to describe time dependent processes. Other testing and associated data reduction procedures have also been employed to study creep crack growth or other stationary loading conditions in bonded joints or laminates (Plausinis and Spelt 1995a, b; Schrader et al. 2022; Jhin et al. 2013; Al-Ghamdi 2004). Various cohesive zone modelling (CZM) techniques has been used for that purpose in order to consider plasticity and/or strain rate and/or temperature effects on the crack propagation conditions (Musto and Alfano 2013; Marquez 2021; Kaminskii 1996; Bradley et al. 1998; Knauss 2015; Miannay 2001; Elmukashfi and Cocks 2017). However, long term crack propagation conditions are rarely investigated. In a previous contribution, an Eulerian description and a finite difference method has been proposed to study crack propagation along a viscoelastic interface (Marquez Costa et al. 2022). With this simple analysis the main features observed during wedge, creep or more classical DCB tests were reproduced. To better understand the influence of viscous phenomena on the slow rate crack propagation in mode I conditions along bonded interfaces, viscoplastic behaviour should also be considered.

In the following, cohesive failure is assumed because it remains a critical condition for sizing of bonded joints (Dillard and Pocius 2002). The crack propagation rate will be controlled by the rheological behaviour of the bonded adhesive layer. The adhesive layer response under mode I loading condition can be described as a whole by introducing an appropriate interface separation law (Dillard and Pocius 2002). An "improved" Nishihara model is then introduced in order to introduce yield stress and nonlinear viscoplastic phenomenon. Using the same combined Eulerian and finite difference resolution technique as proposed by Marquez Costa et al. (2022), the main objective of the present work is to extend it to viscoelasto–viscoplastic bonded interface behaviours. Then a parametric analysis is proposed to outline the correlation between the interface mechanical behaviour and the crack growth kinetics.

## 2 Finite difference analysis of DCB test using Eulerian description

Double cantilever beam (DCB) tests have been proposed for evaluating bonded joint fracture energy (Mostovoy and Ripling 1966). The specimen is produced by bonding together two flexible adherends having rectangular cross section (width: w, thickness: t) as shown in Fig. 1. One end of the specimen is left unbonded along a distance, a, thus forming a pre-crack. Progressive opening displacement is imposed by applying two opposite forces on each adherend at the pre-cracked end of the specimen. From the force vs. opening displacement evolution measured during the crack propagation, the critical SERR of the bonded interface, G_c, is determined. Indeed, simple analytical expressions are found considering approximate expression of the specimen compliance, C, and Irwin–Kies relation (Anderson 2005) in the frame of linear fracture mechanics theory. Thus, assuming the interface compliance is negligible and the adherend deformation is represented with Euler–Bernoulli beam kinematic, the following relations are found:

$$C = \frac{\Delta}{P} = \frac{2a^2}{3EI} \quad G = \frac{a^2 P^2}{wEI}. \tag{1}$$

With E being the adherend Young's modulus and $I = wt^3/12$. Then, assuming no rate dependence due to adhesive or adherend viscosity, the crack propagation is observed when the condition, $G = G_c$, is reached or equivalently when the bending moment in the adherend at crack tip position reaches a critical value:

$$M_c = \sqrt{wEIG_c}. \tag{2}$$

Fig. 1 Schematic representation of a DCB test
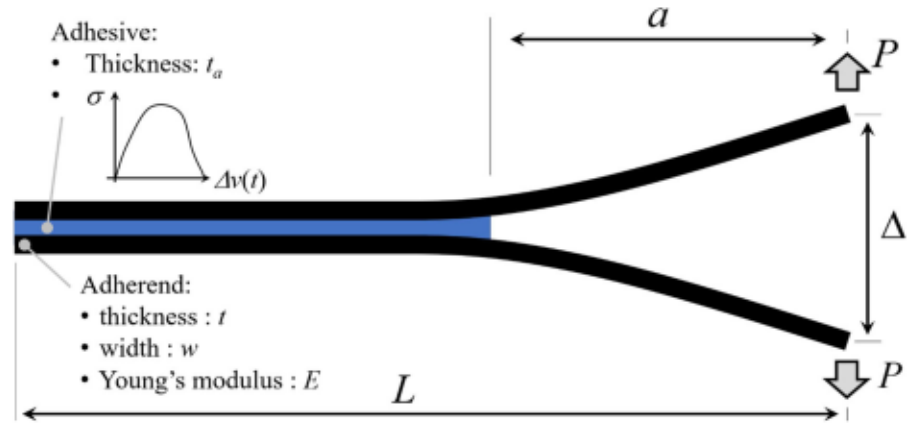
With such a macroscopic approach, the detailed mechanical behaviour of the adhesive layer is not explicitly considered. Additionally, LEFM or NLEFM formulations are not expected to be applicable when viscous and/or rate dependent phenomenon are involved. In the following, a numerical analysis is proposed to study self-similar crack propagation regime along a DCB specimen when the bondline exhibit either viscoelastic or viscoplastic behaviour. As indicated in Sect. 1, the mechanical response of the adhesive layer is considered as a whole using traction–separation approach. Its mechanical behaviour is then described with an appropriate constitutive law controlling the evolution of the local peel stress in the adhesive as a function of the relative displacement between the surface of the adherend in contact with the adhesive layer. As a consequence, possible interphase or adhesion defect effects are not explicitly considered.

2.1 DCB test with viscoelasto–viscoplastic interface/constitutive equations

Since Kanninen's pioneering work (Kanninen 1973), many authors have been interested in more complex traction–separation laws to represent the adhesive layer mechanical behaviours (Musto and Alfano 2013; Blackman et al. 2012; Škec and Alafno 2022; Poblete et al. 2022), including viscous ones (Poblete et al. 2022) trying to reproduce the force vs. opening displacement observed experimentally. The separation between onset, transient and self-similar crack propagation regime was not made despite the distinction introduced in other experimental analysis (Knauss

1973; Liechti and Knauss 1982a, b; Xia et al. 2006). In particular, stationary loading conditions leading to subcritical crack propagation regime were not fully investigated. To determine the relation between specimen loading condition and crack propagation rate in case of self-similar propagation regime, a Eulerian analysis of the DCB specimen is proposed. A finite differences scheme is then implemented to solve both constitutive and equilibrium equations in the process zone region as described in Marquez Costa et al. (2022) and Jumel 2017). Considering Timoshenko beam model can be used to represent the adherend deformation we have:

$$\frac{dM(x)}{dX} + T(X) = 0, \tag{3}$$

$$\frac{dT(x)}{dX} - w\sigma(X) = 0, \tag{4}$$

$$M(X) = EI\frac{d\varphi(X)}{dX}, \tag{5}$$

$$T(X) = \kappa GS\left[\frac{dv(X)}{dX} - \varphi(X)\right], \tag{6}$$

with M, T, φ and v are respectively the local bending moment, shear force, beam cross section rotation and deflection and σ is the local peel stress in the adhesive. E and G are respectively the adherend Young's and shear modulus, $S = wt$ and $I = wt^3/12$ are respectively the adherend cross section and second moment of inertia. Finally, κ is the shear correction factor.

Then, combined viscoelastic–viscoplastic adhesive behaviour is introduced using a 1D Nishihara rheological model to describe the adhesive layer traction–

separation behaviour (Yu et al. 2020) as represented in Fig. 2. The total adhesive deformation is then split into three terms:

$$\varepsilon = \varepsilon_e + \varepsilon_{ve} + \varepsilon_{vp}. \tag{7}$$

ε_e is the reversible elastic contribution, ε_{ve} is the viscoelastic contribution exhibiting delayed effects and time dependent reversible behaviour, finally ε_{vp} is the irreversible contribution which might exhibit rate-dependent effects and progressive irreversible deformation as shown in Fig. 2. The stress vs. strain behaviour of individual components of the rheological model are govern by the following constitutive equations:
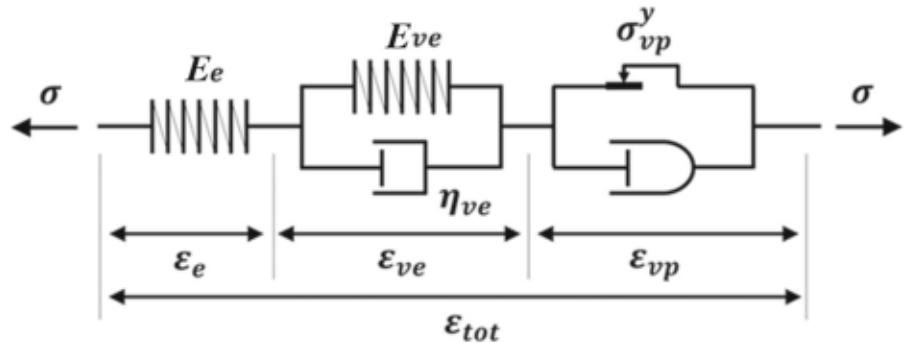
$$\varepsilon_e = \frac{\sigma}{E_e}, \tag{8}$$

$$\sigma = E_{ve}\varepsilon_{ve} + \eta_{ve}\frac{d\varepsilon_{ve}}{dt}, \tag{9}$$

$$\frac{d\varepsilon_{vp}}{dt} = sign(\sigma)\left(\left|\frac{\sigma - \sigma_{vp}}{E_{vp}}\right|\right)^n \quad \sigma > \sigma_{vp},$$

$$\frac{d\varepsilon_{vp}}{dt} = 0 \quad \sigma < \sigma_{vp}. \tag{10}$$

Refined description of the adhesive layer behaviour can be introduced using the same partition using more complex strain hardening law or introducing more terms in the adhesive viscoelastic relaxation spectra. At this stage, a limited number of parameters is introduced to focus only on first order phenomena that are susceptible to control the crack propagation rate. Two situations should be distinguished depending on whether the applied load is more or less than the viscoplastic yield stress σ_{vp}. A straightforward resolution method has been implemented for the purely viscoelastic situation (Marquez Costa et al. 2022)

which is not applicable for the viscoplastic case due to the Boolean condition in Relation (10). The numerical scheme is then modified as follow.

2.2 Combined finite difference: Eulerian resolution technique

The present analysis is limited to the steady state crack propagation regime when the crack propagation rate is supposed to be constant and the fracture process zone (FPZ) configuration is invariant with respect to an observer moving with the crack tip (Fourton 2019). This is a common assumption in many fracture mechanics problems whether dynamic, rate dependent effects, creep behaviour or fatigue loading conditions should be considered and when the FPZ is fully developed.

An Eulerian description of the crack propagation process is then proposed to benefit from the stationary assumption of the FPZ configuration, as shown schematically in Fig. 3. A similar numerical integration scheme can be implemented for the spatial problem related to adherend constitutive and equilibrium equations, but also for the time integration problem describing the Nishihara viscous behaviour. Indeed, the spatial evolution of all mechanical quantities can be related to their time evolution so that:

$$\frac{d.}{dt} = \frac{da}{dt} \cdot \frac{d.}{dX} \tag{11}$$

and the Lagrangian spatial coordinate x is replaced by its Eulerian alternates. Despite, spatial and time numerical integrations are combined, two intricated iterative procedures should be implemented to cope with the highly non-linear nature of the interface behaviour and the coupling between material and structural effects as described below.
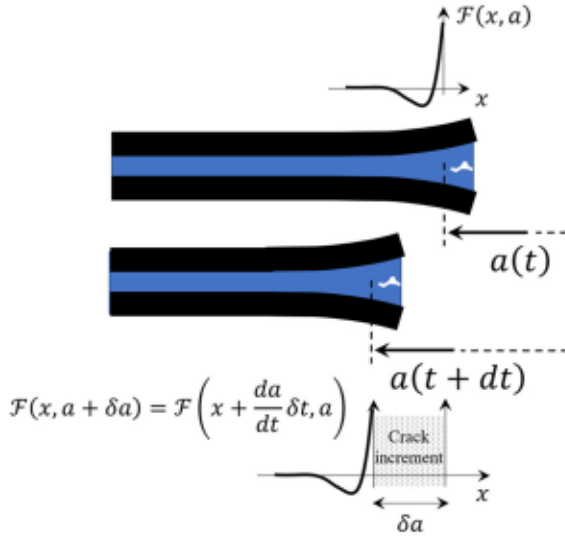
Fig. 2 Rheological diagram for the Nishihara model for a viscoelasto–viscoplastic behaviour

$$\mathcal{F}(x, a + \delta a) = \mathcal{F}\left(x + \frac{da}{dt}\delta t, a\right)$$

Fig. 3 Eulerian description of the crack propagation process

The main iterative procedure is described in Fig. 4. It corresponds to the finite difference implementation of beam equilibrium and constitutive equations (3) to (6). They reduce to two coupled differential equations in, $M(X)$ and $v(X)$:

$$\frac{d^2 M(x)}{dX^2} + w\sigma(X) = 0, \tag{12}$$

$$\frac{d^2 v(X)}{dX^2} - \frac{M(X)}{EI} - \frac{w\sigma(X)}{\kappa GS} = 0, \tag{13}$$

where the peel stress distribution applied to the adherends is supposed to be a known quantity. As proposed in Marquez Costa et al. (2022) and Jumel

(2017), the bonded length of the specimen is discretized in $(N-1)$ regular segments along X with a constant spatial step ΔX, as shown in Fig. 5.

Then, the finite difference method can be applied. The equilibrium and constitutive equations (13) and (14) can be directly solved for any known stress distribution. Thus, consistent deflection and bending moment should be estimated according to the following linear system of equations:

$$\begin{bmatrix} 1 & 0 & -2 & 0 & 1 & 0 \\ 0 & 1 & -\Delta X^2/EI & -2 & 0 & 1 \end{bmatrix} \begin{bmatrix} M_{i-1} \\ v_{i-1} \\ M_i \\ v_i \\ M_{i+1} \\ v_{i+1} \end{bmatrix}$$

$$= \begin{bmatrix} -\Delta X^2 w\sigma_i \\ \Delta X^2 w\sigma_i/\kappa GS \end{bmatrix}. \tag{14}$$

The boundary conditions applicable to DCB test are considered at crack tip position:

$$M(X = 0) = aP \quad T(X = 0) = -\frac{dM}{dX}(X = 0) = P. \tag{15}$$

A semi-analytical solution can be obtained assuming that the bondline behaves elastically so that $\sigma(X) \approx 2E_a v(X)/t_a$, with E_a being the apparent adhesive Young's modulus. The term apparent is used since the adhesive layer is in a confined state. Then, the stiffness connecting the local peel stress to the local relative displacement of adherend normal to the bondline may vary in the interval $[E_a/t_a; E_a(1-v_a)/$
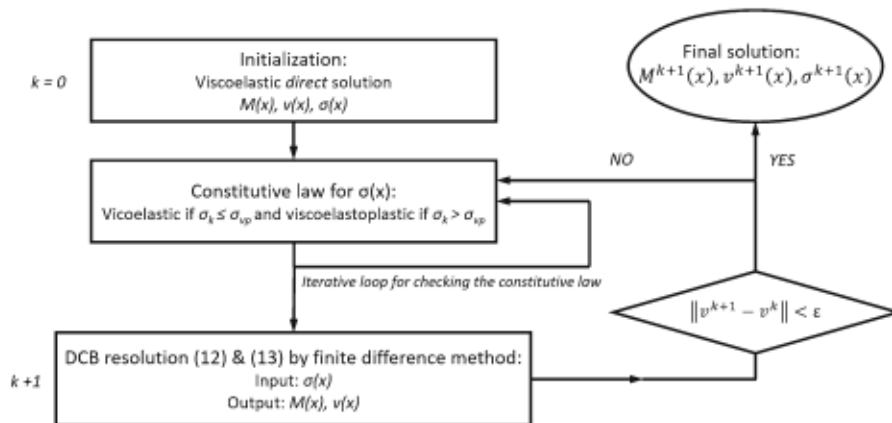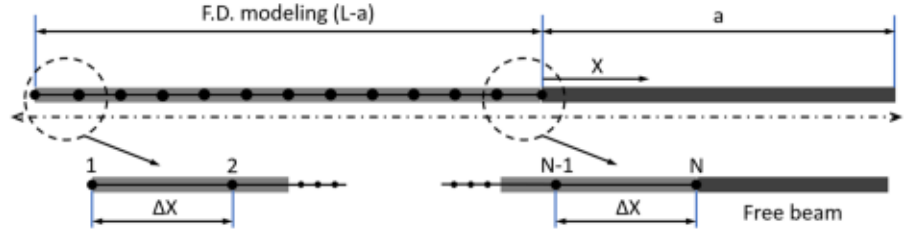

Fig. 4 Flowchart describing the iterative process for computing the DCB response considering a viscoelasto–viscoplastic behaviour of the bonded interface

Fig. 5 1D finite difference modeling of the DCB specimen

$(t_a (1 + v_a)(1 - 2v_a))]$. The elastic solution is used as an initial guess for the iterative process.

Indeed, to cope with the nonlinear viscous behaviour of the bondline, a second iterative procedure is used to re-evaluate at each iteration the peel stress distribution as a function of the actual estimate of the adherend deflection evolution (see Fig. 6). At this step, the Eulerian description is fundamental since it allows a direct correspondence between spatial distribution of the peel strain and stress in the adhesive along the bondline and the loading path in the time domain since $\delta X = da/dt.\delta X$.

The iterative procedure is set as follows. The local adhesive layer peel deformation is determined from the adherend deflection, $\varepsilon = 2v/t_a$. First, the adhesive deformation is supposed to be viscoelastic only (viz. $\varepsilon_{TOT} = \varepsilon_{ve}$). The Boltzmann's superposition principle is then applied to obtain a first estimate of the peel stress evolution:

$$\sigma_B(t) = \int_0^t \mathcal{R}(t - u)d\varepsilon_{ve}(u) \tag{16}$$

with $\mathcal{R}$ being the relaxation function controlling the linear viscoelastic response of the adhesive (Gallegos et al. xxxx). The Expression (16) is more general than the Zener model introduced in the Nishihara model (viz. Figure 2) and allows to introduce a more complex relaxation spectra considering numerous time constant. Then the following steps are repeated to until convergence is achieved on the stress/strain response. First, the viscoplastic contribution on the total deformation is determined from the current peel stress distribution by integrating along the x direction the viscoplastic strain rate evolution using equation:

$$\Delta\varepsilon_{vp}(t) = \int_{-\infty}^0 \frac{1}{da/dt}sign(\sigma)\left(\left|\frac{\sigma - \sigma_{vp}}{K_{vp}}\right|\right)^n (\sigma > \sigma_{vp})dx. \tag{17}$$
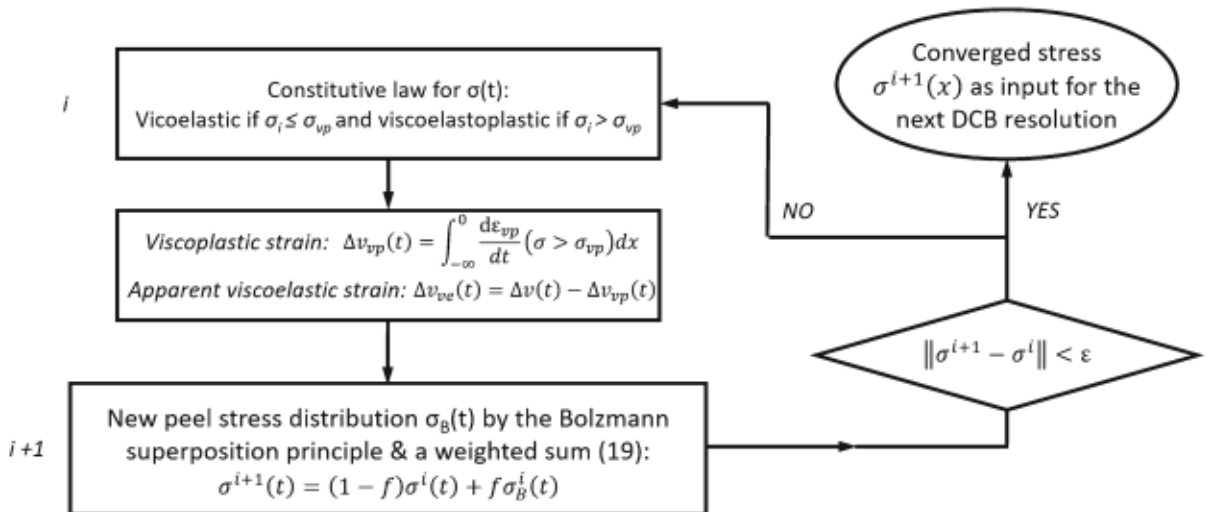
Fig. 6 Flowchart describing the iterative process for checking the viscoelasto–viscoplastic constitutive law and computing the stress distribution along the interface

Then a new estimate of the viscoelastic strain is found with the relation:

$$\Delta\varepsilon_{ve}(t) = \Delta\varepsilon(t) - \Delta\varepsilon_{vp}(t). \qquad (18)$$

The resulting peel stress can be re-estimated again using Boltzmann superposition principle again [viz. Relation (16)] and these steps can be repeated until convergence is reached on $\sigma(t)$ evolution. However, this iterative procedure is highly unstable. Then, for regularization purpose, the peel stress is updated at each iteration using a weighted sum:

$$\sigma^{i+1}(t) = (1-f)\sigma^i(t) + f\sigma_B^i(t). \qquad (19)$$

With $f \approx 0.1$, rapid convergence is found for all tested configurations.

Now that the peel stress distribution has been updated considering the effect of viscoplasticity and viscoelasticity, differential equations (12) and (13) are solved again using the finite difference scheme. These two sequential procedures are repeated iteratively until convergence is achieved in both peel stress and adherend deflection evolutions along the bondline.

Until now, no failure criterion has been introduced. With the traction–separation approach, the crack propagation criterion is defined at the bondline scale by considering ultimate deformation value. A simple failure criterion is used here assuming that the adhesive layer will break when ultimate deformation at break value is reached (viz. $\varepsilon = \varepsilon_{max}$). More sophisticated failure criteria could be introduced, considering the influence of strain rate on the elongation at break for instance, which is out of the scope of the present contribution. Because of the non-linear nature of the problem, a last iterative procedure is then implemented to determine the applied force, P, value leading to the condition, $v = v_{max} = t_a\varepsilon_{max}/2$, at the crack tip position.

3 Effect of interface behaviour on the steady state response

The method presented in Sect. 2 can be used to estimate the stress vs. strain distribution along the process zone during DCB test assuming steady state crack propagation regime. Different interface behaviours can be considered by choosing the appropriate parameters for the Nishihara rheological models

which could lead to extended parametric analysis. However preliminary analysis is proposed here to illustrate the main features obtained from these simulations but also to compare slow rate crack propagation conditions caused either by viscoplastic or viscoelastic bondline behaviours. In the following, the same adherend characteristics will be used for all simulation as indicated in Table 1.

3.1 Viscoelastic interface behaviour

At first, the Nishihara model is reduced to a simple Zener viscoelastic model. The viscoelastic behaviour is then driven by two characteristic times (creep: τ_c, relaxation: τ_r) and one elastic modulus, or equivalently by one time constant and the glassy, E_0, and rubbery, E_∞, moduli. A set of arbitrary parameters has been chosen (see Table 2) so as to exhibit significant drop of the moduli, $E_0/E_\infty = 5$.

For dimensional analysis purposes, the parameter:

$$\lambda = \sqrt[4]{\frac{E_a}{t_a EI}} \qquad (20)$$

is introduced. This wavenumber controls the extent of the process zone ahead the bondline edge. Due to the viscoelastic nature of the adhesive "Young's modulus", E_a, is not a constant value and varies in the interval $[E_\infty, E_0]$. In the following, the rubber stiffness $E_a = E_\infty$ will be used to evaluate λ since it is related to largest process zone length. The set of parameters has been chosen so that for crack propagation rate value below $1e^{-3}$ mm s^{-1}, viscoelastic effect is expected by simply considering that when the time needed for the crack to propagate over a distance $2\pi.\lambda^{-1}$ [viz. $t \approx 2\pi.\lambda^{-1}/(da/dt)$] is more than τ_c, the adhesive is susceptible to exhibit viscoelastic creep response.

The theoretical stress/strain evolution resulting from constant strain rate loading condition is presented in Fig. 7. An arbitrary 8% ultimate strain value will be considered in the following as failure criteria for the theoretical analysis. From these theoretical calculations, a significant apparent stiffness variation is observed in the range 10^{-7}s$^{-1} < \dot{\varepsilon} < 10^{-3}$s^{-1} where viscous dissipation is maximized.

Using the numerical implementation detailed in Sect. 2, the peel strain and peel stress time and spatial evolutions in the adhesive along the bondline can be determined considering various crack propagation
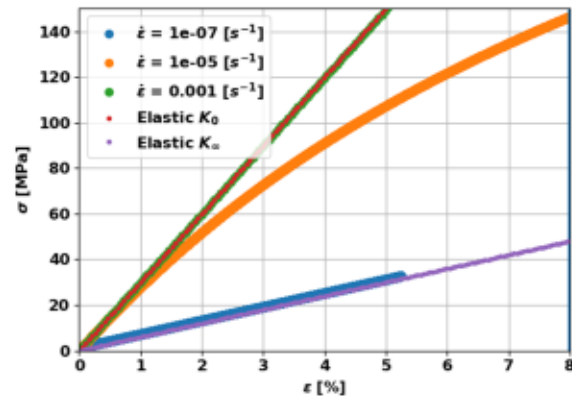
Table 1 Adherend material properties and geometrical parameters of the DCB specimen

w (mm)	t (mm)	L (mm)	A (mm)	E (GPa)	v	t_a (µm)
25	5	150	30	70	0.3	500

Table 2 Viscoelastic properties

| E_e (MPa)	E_∞ (MPa)	E_{ve} (MPa)	τ_c (h)	τ_r (h)
3000	600	750	7.29	1.46

Fig. 7 Stress vs. strain response assuming a viscoelastic adhesive behaviour for different $\dot{\varepsilon}$

rates but the same propagation condition, $v = v_{max} = 20$ µm, at the bondline edge. These results are reported in Fig. 8 for crack propagation rate ranging in the interval $[0.0001\ 2].1e^{-3}$ mm/s. To exhibit dimensionless quantities, the parameter, λ, is used as reference wavenumber value, and the creep time, τ_c as a reference time. The numerical evaluation of the FPZ configuration does not reveal any significant feature related to the viscoelatic nature of the bondline. Indeed, as for the elastic situation, pseudoperiodic evolutions of peel stress and strain along X are observed for all da/dt values considered here. The process zone extent does not vary much compared to the two limit cases corresponding to glassy and relaxed behaviours. It should be noticed here that despite a significant evolution of the Young's modulus, the variation of the extent of the process zone between glassy and relaxed state, as estimated from the λ value, is only 50% (see Fig. 8, Elastic E_0 vs. Elastic E_∞). It should be noted, however, that the

maximum compressive strain reaches peak value in the intermediate crack propagation range while the minimum value normalized stress distribution (σ/σ_{max}) remains unchanged. The evolution of dv/dX along the process zone is also plotted in Fig. 8b to evidence whether the viscous behaviour of the bondline may produce a significant variation of the adhesive deformation rate profile along the bondline. The evolutions are very similar, which indicate that the adhesive strain rate relative variation along the bondline is unchanged, but its amplitude is mostly driven by the crack propagation rate rather by a complex coupling between the adherend deformation and viscoelastic behaviour of the adhesive. To show more clearly the influence of adhesive viscoelastic behaviour, the peel stress is plotted as a function of peel strain for various crack propagation rates (see Fig. 8d). It should be noted here that these evolutions differ from the ones presented in Fig. 7 representing the viscoelastic response under constant deformation rate. Due to the viscoelastic behaviour, the material stiffness drops when the crack propagation rate decreases. More interestingly, it can be observed that due to the loading history and toggling between compression and tensile states with varying strain rate, a hysteretic loop is observed in a transition regime between fast and slow propagation rate corresponding respectively to glassy and rubbery behaviour. In this intermediate crack propagation regime, the viscous dissipation will then be amplified making the condition for a crack to propagate more severe. The applied force, P, that provokes crack propagation can be determined from the simulations. These results will be presented and discussed in Sect. 3.

3.2 Viscoplastic interface behaviour

For viscoplastic materials and for highly deformable adhesives, significant irreversible creep deformation might be observed once a threshold applied stress value is reached (Miannay 2001). Under stationary loading condition, continuous progressive and
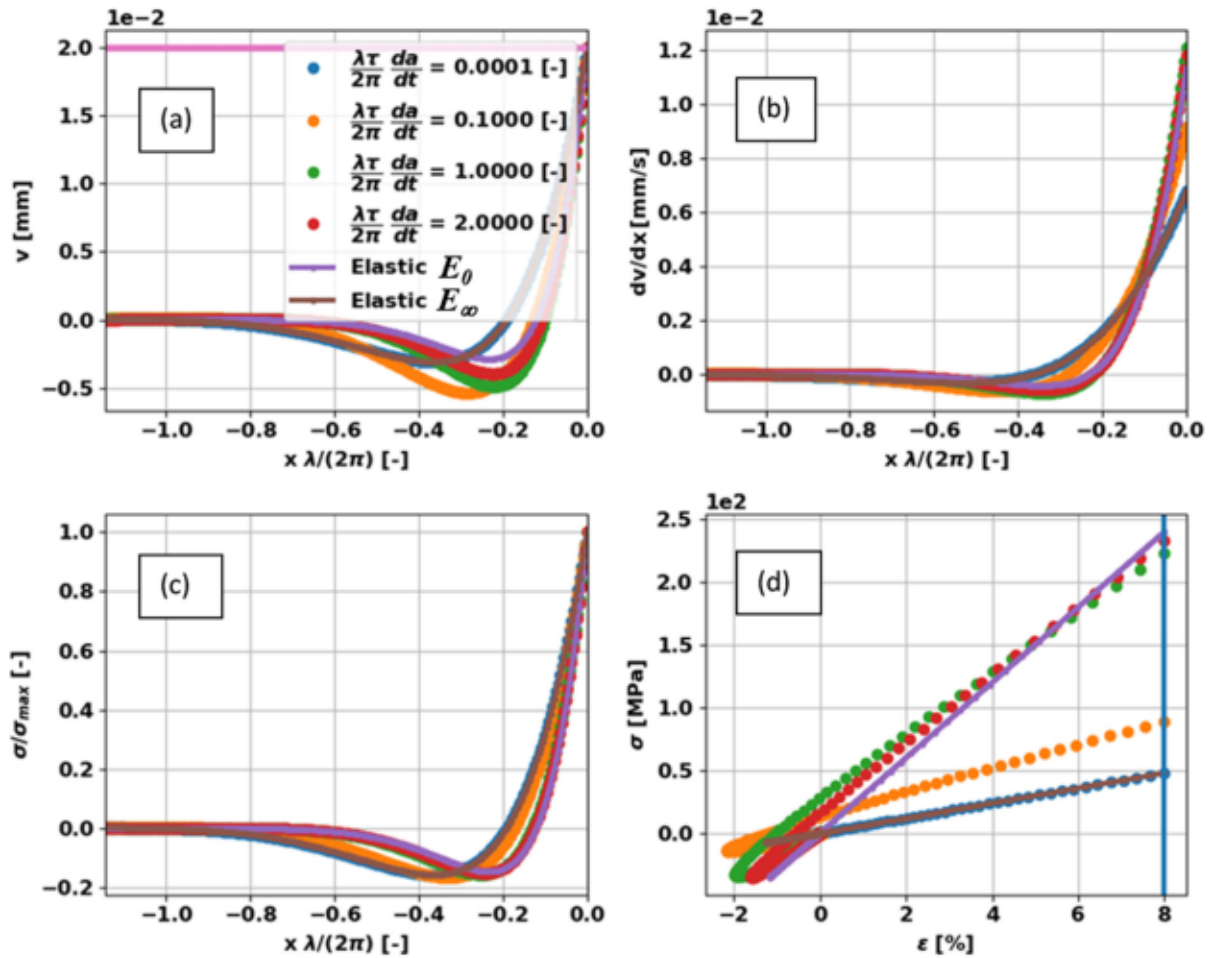
Fig. 8 Evolution of **a** adherend deflection, **b** adherend deflection rate, **c** normalized peel stress and **d** peel stress vs. peel strain ahead the crack tip along viscoelastic interface for various dimensionless crack propagation rate 0.0001, 0.1, 1 and 2 [–] (equivalent to $1e^{-7}$, $1e^{-4}$, $1e^{-3}$ and $2.1e^{-3}$ mm/s) and purely elastic behaviour

irreversible deformation is observed revealing the viscoplastic nature of such materials. However, these time/strain rate dependent dissipative mechanisms are rarely evaluated explicitly in the global energy balance analysis leading to critical SERR evaluation (Nicolas and Jumel 2016). As for the viscoelastic situation, the numerical procedure detailed in Sect. 2 is used to evaluate the evolutions of peel stress and peel strain along the process zone and as a function of time. A first set of material parameters have been set arbitrary to observe some possible coupling between viscoplastic and viscoelastic contributions in the transition regime between fast and slow crack propagation regime. While the adherend parameters and the viscoelastic properties are kept the same, an additional viscoplastic contribution is added in the Nishihara model

considering the set of parameters: $n = 1$, $E_{vp} = 10^{-1}$ η_{ve}, $\sigma_{vp} = 30$ MPa.

Figure 9 presents the theoretical stress vs. strain evolutions under constant deformation rate for the theoretical viscoelastic-viscoplastic Nishihara model. Significant strain rate dependence is observed with both viscoelastic and viscoplastic effects in the range $1.e^{-7}\mathrm{s}^{-1} < \dot{\varepsilon} < 1.e^{-3}\mathrm{s}^{-1}$. For high strain rate conditions, the response is mainly elasto–viscoplastic. The "apparent" Young's modulus remains constant, $E_a \approx E_0$. When, $\sigma > \sigma_{vp}$, plastic behaviour is observed whose strain rate dependence is govern by the Norton's law. Finally, for slow deformation rates, the initial apparent elastic modulus decreases due to viscoelastic relaxation until $\sigma > \sigma_{vp}$ and the material starts to flow. This indicates possible complex
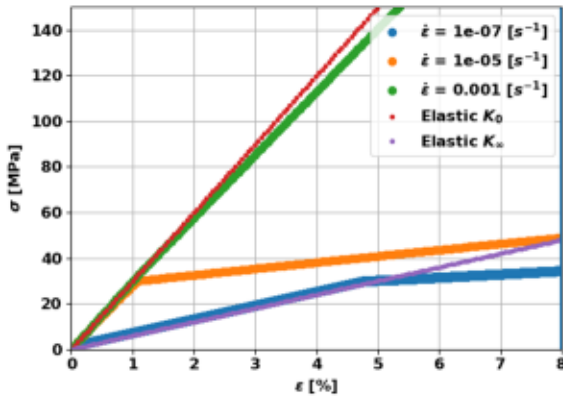
Fig. 9 Theoretical stress vs. strain evolution under constant deformation rate condition for the viscoelastic–viscoplastic theoretical adhesive behaviour

coupling could occur between viscoelastic and viscoplastic contributions.

Now, the additional coupling with adherend deformation should be examined when considering the self-similar crack propagation along the bondline. The numerical procedure presented in Sect. 2 is used again to determine the stress vs. strain distribution along the bondline for various crack propagation rate values and considering the full viscoelastic–viscoplastic adhesive layer behaviour. The same results as the ones discussed in the previous section are presented in Fig. 10 which to exhibit specific features along the process zone which could reveal the viscous (viscoplastic or viscoelastic) nature of the adhesive bondline. A clear modification of the process zone configuration as a function of the crack propagation rate is observed again. However, the evolution of adhesive strain (or equivalently adherend deflection) along the bondline is very similar to the purely elastic situation again. The pseudoperiodic attenuation is controlled again by the average apparent stiffness of the bondline along the process zone due to coupling with adherend deformation. Weak variation of dv/dx evolution along the bondline is observed which suggests again that the strain rate loading condition is mostly controlled by the crack propagation rate. The effect of viscoplasticity is more visible on the evolution of the peel stress along the adhesive. Indeed, a plastic process zone is clearly visible for medium to low crack propagation rates where viscoplastic flow

limits the maximum peel stress value ahead of the bondline edge. Finally, the peel stress versus peel strain evolution evidences the complex situation to be considered to analyze slow rate crack propagation phenomenon when both viscoplastic and viscoelastic dissipation mechanisms are involved. As for the situation depicted in Fig. 9, strain rate dependence is evidenced by the increase of adhesive layer stiffness and hardening with the crack propagation rate. However, an additional hysteretic loop is also seen due to the compression/tension loading sequence. While viscoplastic and viscoelastic contributions were activated sequentially in Fig. 9 they are both visible at a given crack propagation rate due to significant variation of the strain rate along the bondline.

3.3 Focus of viscoplastic contribution to the mechanical response

The complex situation described above cannot be generalized since the results are obtained with a given arbitrary set of parameters. Rather than performing an extensive parametric analysis, we now focus on the only viscoplastic behaviour attempting to exhibit specific features either at a macroscopic or a local scale which could be distinguished from the ones observed in viscoelastic situation. Then, the Nishihara model is reduced to only elastic and viscoplastic contributions. The elastic Young's modulus is set to E_0, for the viscoplastic part, the same Norton's law parameters as before are kept. The resulting stress/strain evolution under constant deformation rate condition are presented in Fig. 11. As expected, no rate dependence is observed below the plastic threshold σ_{vp}. Then, plastic flow is observed with strain rate hardening effect. For very high deformation rate, quasi elastic behaviour is observed.

Then, numerical simulations have been carried out for DCB configuration considering the same viscoplastic interface behaviour but also the same failure criterion, $v_{max} = 20$ μm, as the one used in the previous section. Figure 12 shows the resulting peel strain, the strain rate and peel stress evolutions along the bondline for various crack propagation rates (0.0001, 0.01, 0.1 and 2) $1e^{-3}$ mm/s and assuming self-similar crack propagation. Also, the stress vs. strain evolution at the bonded interface is reported.
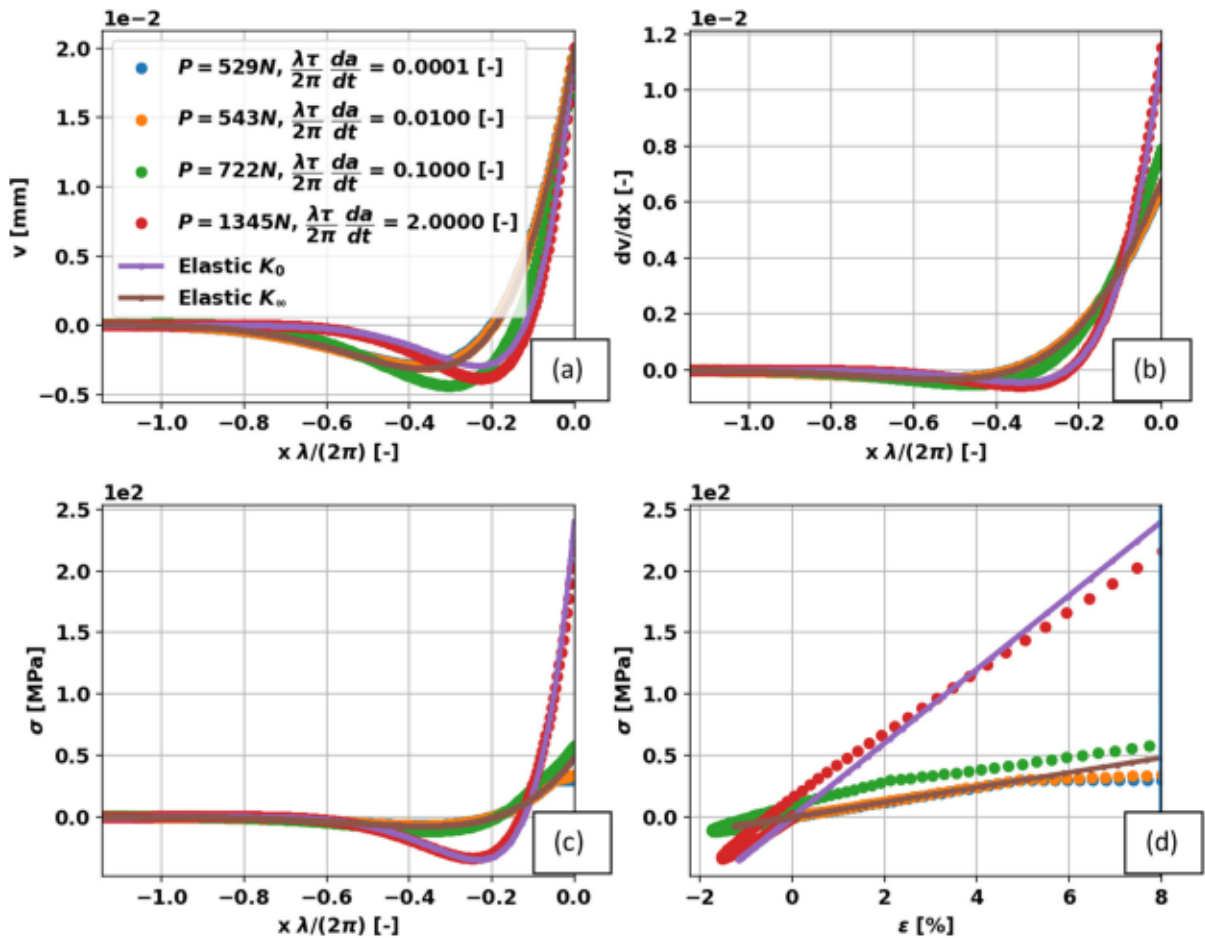
Fig. 10 Evolution of **a** adherend deflection, **b** first derivative of adherend deflection, **c** peel stress along the adhesive layer, and **d** resulting peel stress vs. peel strain evolution in the adhesive layer during crack propagation. Viscoelastic–viscoplastic adhesive behaviour for various crack propagation rate of 0.0001, 0.01, 0.1 and 2 [–] (equivalent to $1e^{-7}$, $1e^{-5}$, $1e^{-4}$ and $2.1e^{-3}$ mm/s)
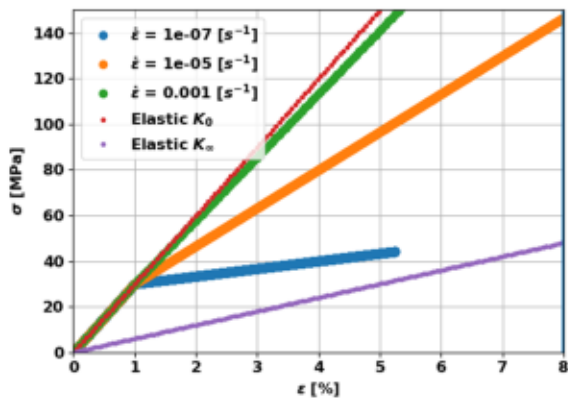
Fig. 11 Theoretical stress vs. strain evolutions under constant deformation rate, viscoplastic case

The description of the process zone is rather straightforward here. Indeed, with respect to the resulting stress vs. strain evolution, its distribution along the bondline for a given crack propagation rate is similar to the one observed for an elasto–plastic adhesive with linear hardening (see Fig. 12). The plastic zone extension ahead of the crack tip is small compared to the whole process zone length so that in this region the strain rate variation is negligible. The resulting stress vs. strain evolution is similar to the one observed under constant strain rate condition. While the crack propagation rate affects the whole strain/ stress evolutions along the bondline in case the viscoelastic behaviour, it only affects the small region close to the bondline edge in the viscoplastic situation.
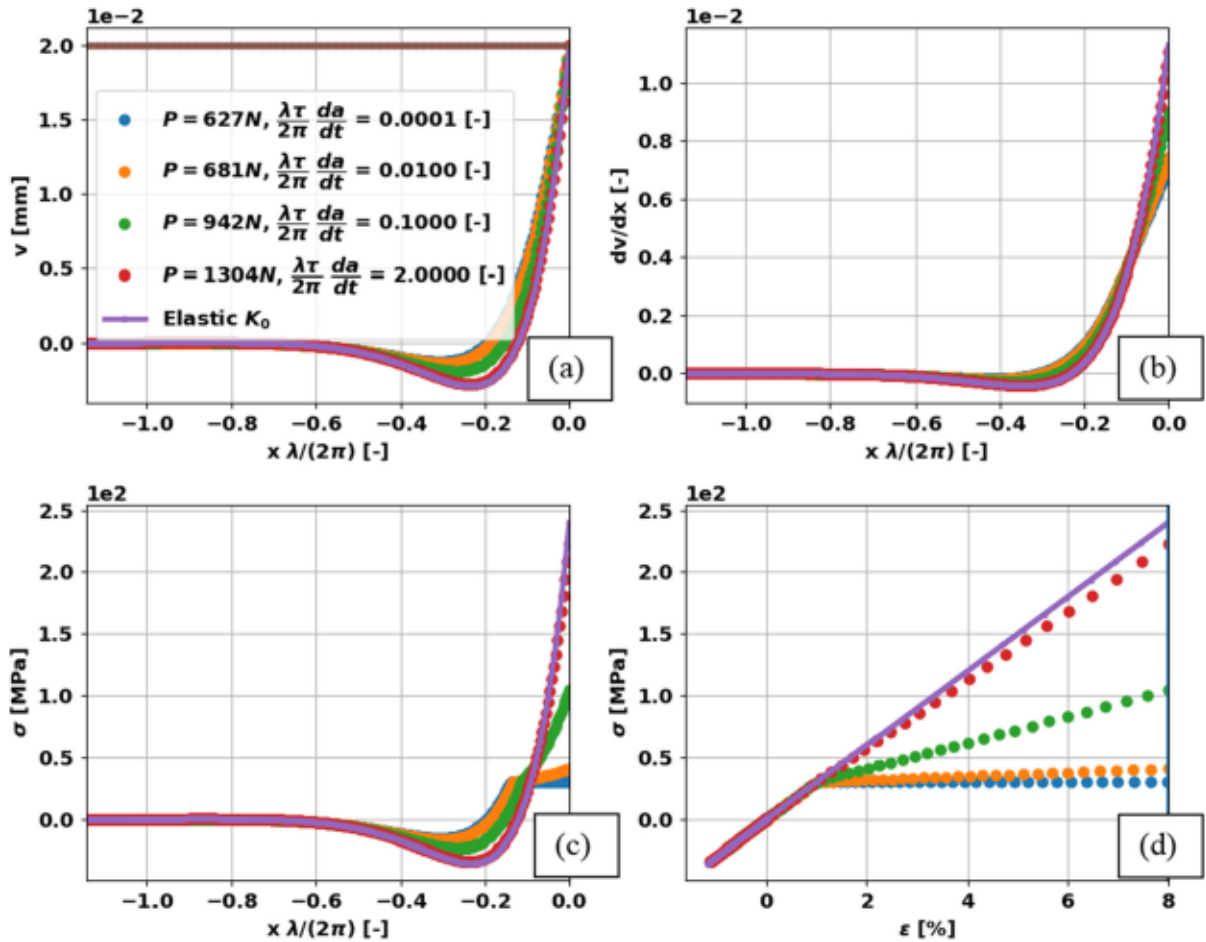
Fig. 12 Evolutions of **a** adherend deflection, **b** first derivative of adherend deflection, **c** peel stress along the bondline, and **d** peel stress vs. peel strain evolution. Viscoplastic bondline behaviour for various crack propagation rate of 0.0001, 0.01, 0.1 and 2 [–] (equivalent to $1e^{-7}$, $1e^{-5}$, $1e^{-4}$ and $2.1e^{-3}$ mm/s)

4 Fracture durability in viscous and plastic media

The previous analyses focus on the only description of stress vs. strain distribution along the process zone trying to distinguish viscoelastic from viscoplastic situation. Now considering an identical failure criterion at the bondline scale, $v = v_{max}$, the macroscopic loading conditions leading to crack propagation will be determined as a function of the crack propagation rate. As discussed in Sect. 2, the SERR is generally used to describe crack propagation onset condition in the frame of LEFM. When time dependent behaviours are involved, other macroscopic time dependent quantities such as C^*, J_v, C_v, H, M_θ, etc. have been also proposed to exhibit mechanical quantities which drive the crack propagation process (Broughton and

Mera 1997; Ji et al. 2004). They are applicable when the medium surrounding the FPZ exhibit time-dependent behaviour. These mechanical quantities should be correlated to material parameters or master curve driving the fracture process at the local scale or at a macroscopic scale. In the framework of the present analysis, the SERR is relevant as a driving parameter since the adherends surrounding the process zone are linear and elastic. As proposed in other contribution (Plausinis and Spelt 1995a, b; Jhin et al. 2013; Broughton and Mera 1997) dealing with Boeing Wedge test analysis for instance, the instant SERR value, G, drives the crack propagation rate da/dt, as described by a "pseudo-master" curve describing the evolution of the critical SERR as a function of strain rate $G_c(da/dt)$. As evidenced in the previous sections,

the process zone configuration will change with the crack propagation rate so as different crack length correction values should be used for proper evaluation of G. For the sake of simplicity, the results of all calculations will be presented in a more straightforward manner by representing the evolution of the crack propagation rate as a function of applied bending moment at crack tip position as given by Relation (2). This relation is based only on simple beam theory so that the additional compliance due to FPZ finite length is not considered by using crack length correction for instance. The transverse force, P, so as the bending moment, $\underline{aP}$, may also contribute to the crack propagation process when the crack length value, a, is small. However, the present contribution essentially focuses on the evaluation of the dependence of G_c dependence on the crack propagation rate, da/dt, rather than evaluation of the SERR itself. Then, several series of calculations are performed to evaluate not only the influence of bending moment but also the transverse force by considering different crack length values. Pure viscoelastic then viscoplastic behaviours are studied successively considering the simple $v = v_{max}$ failure criteria. The resulting "master curves" are reported in Figs. 13 and 15. For each configuration, two limit configurations can also be reported corresponding to slow and fast strain rates where the stress versus strain evolution along the process zone is identical to the one determined under constant strain rate condition. Then the critical SERR can be determined with the relation:

$$G_c = t_a \int_0^{\varepsilon_{max}} \sigma(\varepsilon)d\varepsilon, \tag{21}$$

For both viscoelastic and viscoplastic situations G_c varies in the interval $[G_c^{min} \quad G_c^{max}]$ corresponding respectively to slow and fast crack propagation rate conditions. The corresponding critical bending moments, M^{max} and M^{min}, are obtained from Relation (2).

In Fig. 13, the results obtained for viscoelastic interface are reported for 5 crack length values (30 mm to 300 mm). The smallest crack length value is close to FPZ size, while for the larger one the contribution of interface deformation on the specimen compliance becomes very weak. As observed before, two limit situations can be reported corresponding to very fast and very slow rate crack propagation conditions. Indeed, in both cases no strain rate effect is observed at the process zone scale and the resulting interface behaviour can be reduced to an elastic one. Accordingly, the critical bending moments for fast and slow crack propagation rate conditions are driven by the critical SERR determined with the high and slow deformation rate assumption (see black lines), respectively. These values overestimate the ones obtained for all test cases. Indeed, for correct evaluation of the SERR, crack length correction, a_c, should be added to the geometrical one so that:

$$a_c = \left(\frac{M_c^{th}}{M_c} - 1\right)a \tag{22}$$

Fig. 13 Crack propagation rate (logarithmic scale) as a function of applied moment for different initial crack lengths for viscoelastic interface behaviour
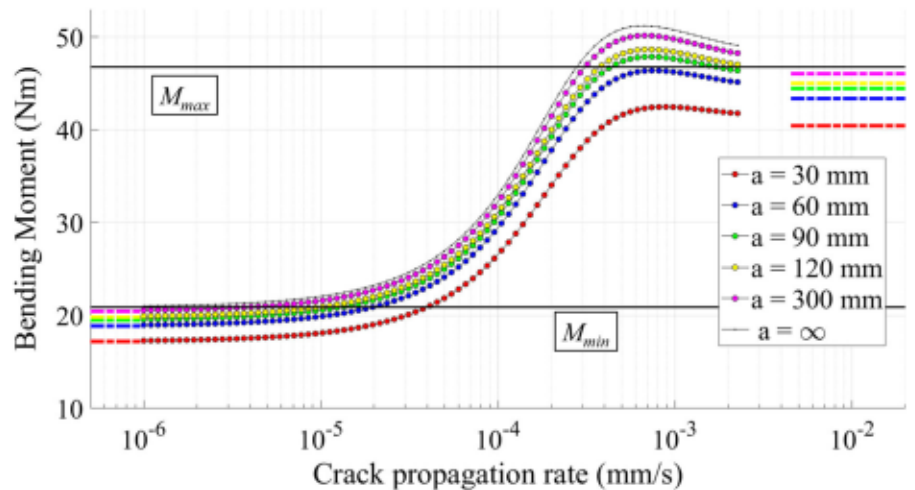
with M_c^{th} and M_c being, respectively, the critical bending moment for rigid and soft interface. Adding a crack length correction reflects the influence of the bondline compliance. The critical bending moment is evaluated for each a value by using a beam on an elastic foundation (BEOM) model as presented in Jumel et al. (2013). Asymptotic evolutions coincide with the values predicted with this simple model which assesses the use of simple elastic foundation correction for slow and fast rate crack propagation regimes. In the interval 10^{-5} mm/s $<$ da/dt $< 10^{-3}$ mm/s a rapid variation of applied bending moment is observed mostly due to the increase of interface stiffness due to the increase of strain rate. With the failure condition $v = v_{max}$, the adhesive is then capable to store more potential energy before failure occurs with increasing crack propagation rate. Also, a peak bending moment value is observed above the expected critical value before the plateau value associated with fast crack propagation rate regime. This unexpected result is attributed to the presence of the hysteretic loop in the stress vs. strain evolution for a specific crack propagation range. This induces supplementary viscoelastic dissipation leading to higher applied bending moment.

Finally, crack propagation rate dependent crack length correction is introduced in an attempt to build a unique "master curve". Applying Relation (22) for all crack propagation rate conditions, the crack length correction and critical bending moment value can be determined. Resulting M_c^{th} evolution is also reported in Fig. 13. For slow and fast crack propagation rate values, the asymptotic evolutions correspond to the ones predicted with the SBT theory. This M_c^{th} corresponds to the one obtained under pure bending moment loading condition. The evolution of the crack length correction value, a_c, is reported in Fig. 14. It should be noted that the same values are found for all crack length values considered in the simulation so that no approximation is made here. As expected the crack length correction varies with the crack propagation rate due to the viscoelastic nature of the interface. For both slow and fast crack propagation rates, the correction is equal to the one predicted with the simple beam on elastic foundation approximation. In the intermediate regime the crack length correction decreases after a small overshot is found when maximum G_c value is found.

Figure 15 shows the critical bending moment vs. crack propagation evolutions obtained when considering viscoplastic bondline behaviour. Results are very similar to the ones obtained for the viscoelastic case with a marked transition between slow crack propagation to fast crack propagation rates. Again, two asymptotic situations are observed which can be easily predicted by considering the adhesive stress vs strain evolution under high and slow strain rate loading conditions. Contrary to the viscoelastic situation no peak critical bending moment value is observed but monotonous evolution due to increasing viscoplastic dissipation with the strain rate and
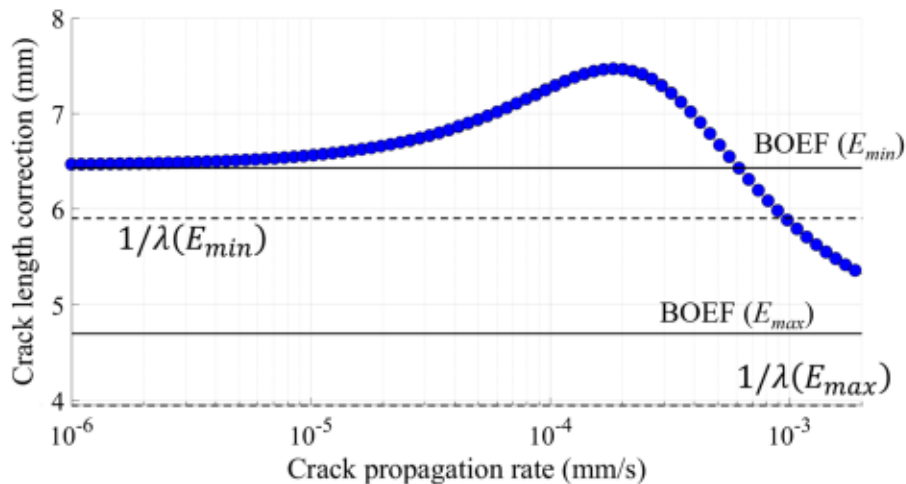
Fig. 14 Crack propagation rate dependence of the crack length correction value. Comparison with beam on elastic foundation (BOEF) estimation, and process size extend ($1/\lambda$)

Fig. 15 Crack propagation rate (logarithmic scale) as a function of applied moment for different initial crack lengths for viscoplastic interface behaviour
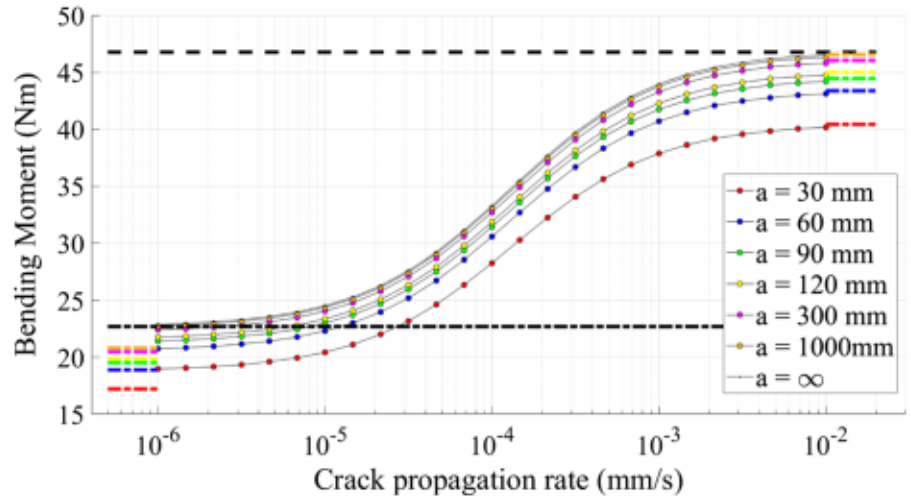
presence of viscoplasticity ahead of the bondline edge only. The same BOEF approximation is used to predict the asymptotic values for various considered crack length values. Contrary to the viscoelastic situation, the slow rate crack propagation regime doesn't match with predicted behaviour due to the presence of a plastic zone region ahead the crack tip.

Then, the same methodology as the one proposed for the viscoelastic case is used. For each crack propagation rate critical bending moment M_c^{th} and crack length correction value, a_c, are determined with the Relation (22). $M_c^{th}(da/dt)$ "master curve" is reported in Fig. 15 and the evolution of crack length correction as a function of the crack propagation rate is reported in Fig. 16. Due to the reconfiguration of the FPZ, a smooth increase of the crack length correction

is observed in the intermediate crack propagation rate regime due to the progressive extension of the plastic zone. Again, the same crack length correction value is found for all considered crack length values. This parameter is controlled by the FPZ configuration which is essentially controlled by the applied bending moment at crack tip position.

5 Conclusions and perspectives

The present work aims to evaluate the role of the bonded interface time-dependent rheological behaviour on the crack propagation conditions during DCB test under stationary loading conditions. A specific numerical scheme has been implemented considering

Fig. 16 Evolution of the crack length correction value as a function of crack propagation rate. Comparison with BOEF estimate, evidence of plastic zone extension
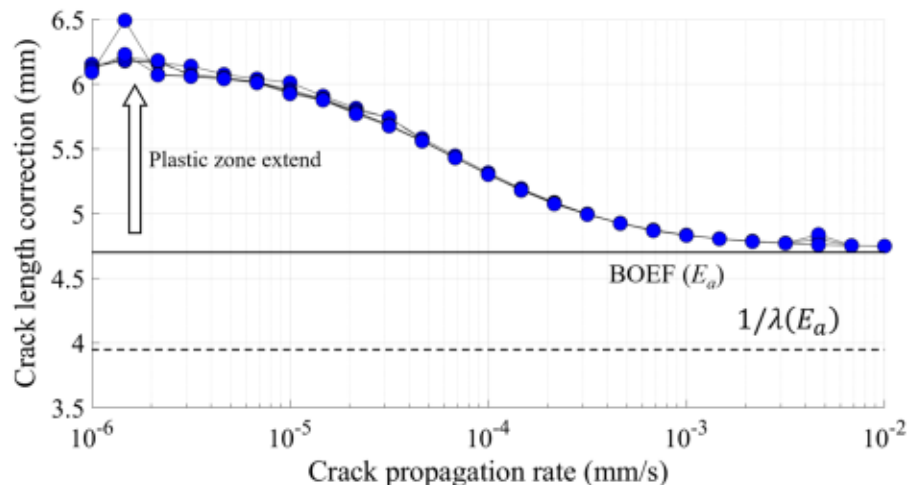
steady-state crack propagation conditions and considering the viscous nature of the bondline. A Eulerian approach is used to reduce the complex time and space integration procedure to only a spatial one using finite difference method. Combination of elastic, viscoelastic, elasto–viscoplastic contributions can be considered at the interface scale using an improved Nishihara model. The viscoelastic and viscoplastic bonded interface behaviours are then compared. At the process zone scale, significant differences are observed on the strain and stress spatial and time evolutions. At macroscopic scales, "master curves" are obtained by plotting crack propagation rate, da/dt, as a function of driving bending moment at the crack tip position. Similar evolutions are observed for both viscoelastic and viscoplastic cases. These evolutions can be bounded by considering two limit situations and using simple LEFM analysis. However, a peak critical bending moment is observed for the viscoelastic evidencing crack propagation rate range where viscoelastic dissipation is more pronounced. No such effect is observed for the viscoplastic situation. For a unique master curve to be obtained, when DCB specimen is used corresponding to the application of a transverse force at a finite distance from the bondline, a crack length correction coefficient must be introduced. This quantity is also crack propagation rate dependent but is found stationary for all considered crack length values thus revealing the universal nature of the resulting master curve.

This preliminary analysis provides interesting insight on the role of the respective contributions of viscoelastic and viscoplastic dissipation on the slow rate crack propagation conditions considering time-dependent bonded interface behaviour. However, some additional analysis should be engaged to provide a more straightforward estimate of the crack length correction values. Also, while more complex time-dependent behaviour can be considered with the proposed model, only pure viscoelastic or viscoplastic behaviour is studied here. Supplementary analysis is now in progress to evaluate possible coupling between viscoelastic and viscoplastic contributions to implement more complex relaxation spectra or viscoplastic behaviour or introduce rate dependent damage in the FPZ. These simulations will be useful for proposing adequate methodology to estimate the long-term failure behaviour of adhesively bonded joint submitted to creep loading conditions. This theoretical/

numerical framework should be used with recent experimental set-up in order characterize at global and local scale the creep crack growth conditions. Pulley based systems which are able to apply pure bending moments (Carreras et al. 2023) are the most adequate since the loading conditions are identical to ones used to establish the master curves.

References

Al-Ghamdi AH (2004) Fatigue and creep of adhesively bonded joints. Doctoral Dissertation, Loughborough University

Anderson TL (2005) Fracture mechanics: fundamentals and applications. Taylor & Francis Group, New York

Barla G, Debernardi D, Sterpi D (2012) Time-dependent modeling of tunnels in squeezing conditions. Int J Geomech 12(6):697–710

Blackman BRK, Kinloch AJ, Rodriguez-Sanchez FS, Teo WS (2012) The fracture behaviour of adhesively-bonded composite joints: effects of rate of test and mode of loading. Int J Solids Struct 49(13):1434–1452

Bradley W, Cantwell WJ, Kausch HH (1998) Viscoelastic creep crack growth: a review of fracture mechanical analyses. Mech Time Depend Mater 1:241–268

Broughton WR, Mera RD (1997) Review of durability test methods and standards for assessing long term performance of Adhesive Joints. Technical Report. National Physical Laboratory, Teddington

Budzik M, Jumel J, Imielińska K, Shanahan MER (2009) Accurate and continuous adhesive fracture energy determination using an instrumented wedge test. Int J Adhes Adhes 29(7):694–701

Carreras L, Bak BLV, Jensen SM, Lequesne C, Xiong H, Lindgaard E (2023) Benchmark test for mode I fatigue-driven delamination in GFRP composite laminates: experimental results and simulation with the inter-laminar damage model implemented in SAMCEF. Composites B 253:110529

Dillard DA, Pocius AV (2002) The mechanics of adhesion. In: Adhesion science and engineering—1. Elsevier, Amsterdam

Elmukashfi E, Cocks AC (2017) A theoretical and computational framework for studying creep crack growth. Int J Fract 208(1):145–170

European Cooperation for Space Standardization (ECSS) (2011) Space engineering. In: Adhesive bonding handbook. ECSS Secretariat ESA-ESTEC, Requirements and Standards Division, Noordwijk

Fahimifar A, Karami M, Fahimifar A (2015) Modifications to an elasto–visco-plastic constitutive model for prediction of creep deformation of rock samples. Soils Found 55(6):1364–1371

Fourton P (2019) Dynamic adhesion breaking in laminated glass—effect of interfaces and polymer's rheology. Chemical Physics [physics.chem-ph]. Université Paris sciences et lettres, France

Gallegos C, Martinez Boza JF (N.D.) Linear viscoelasticity. In: Rheology, vol 1. UNESCO-EOLSS

Holmes DW, Loughran JG, Suehrcke H (2006) Constitutive model for large strain deformation of semicrystalline polymers. Mech Time Depend Mater 10(4):281–313

Jhin G, Azari S, Ameli A, Datla NV, Papini M, Spelt JK (2013) Crack growth rate and crack path in adhesively bonded joints: comparison of creep, fatigue and fracture. Int J Adhes Adhes 46:74–84

Ji SS, Genin GM, Paris PC, Berkel TR, Rubin AM (2004) Polymer/metal interfacial crack growth characterized by C. Int J Fract 129(1):63–73

Jumel J (2017) Crack propagation along interface having randomly fluctuating mechanical properties during DCB test finite difference implementation—evaluation of G_c distribution with effective crack length technique. Composites B 116:253–265

Jumel J, Budzik MK, Salem NB, Shanahan MER (2013) Instrumented end notched flexure-crack propagation and process zone monitoring. Part I: modelling and analysis. Int J Solids Struct 50(2):297–309

Kaminskii AA (1996) Modeling quasistatic fracture at a crack tip in polymers and composites under long-term loading. Int Appl Mech 32(7):493–517

Kanninen MF (1973) An augmented double cantilever beam model for studying crack propagation and arrest. Int J Fract 9:83–92

Knauss WG (1973) On the steady propagation of a crack in a viscoelastic sheet: experiments and analysis. In: Kaush HH, Hassel JA, Jaffee RI (eds) Deformation and fracture of high polymers. Plenum Press, New York

Knauss WG (2015) A review of fracture in viscoelastic materials. Int J Fract 196:99–146

Liechti KM, Knauss WG (1982a) Crack propagation at material interfaces: I. Experimental techniques to determine crack profiles. Exp Mech 22(7):262–269

Liechti KM, Knauss WG (1982b) Crack propagation at material interfaces: II experiments on mode interaction. Exp Mech 22:383–391

Majda P, Skrodzewicz J (2009) A modified creep model of epoxy adhesive at ambient temperature. Int J Adhes Adhes 29(4):396–404

Marquez Costa JP (2021) Characterisation and modeling of interfaces in laminated organic composites at high temperature—application to fire resistance of aeronautical structures. PhD Thesis, Paris Saclay University, France

Marquez Costa JP, Jumel J, Badulescu C, Stamoulis G (2022) Self-similar crack propagation along viscoelastic interface during double cantilever beam test. Mech Time Depend Mater. https://doi.org/10.1007/s11043-022-09559-8

Miannay DP (2001) Time-dependent fracture mechanics. Mechanical engineering series. Springer, New York

Mostovoy S, Ripling EJ (1966) Fracture toughness of an epoxy system. J Appl Polym Sci 10(9):1351–1371

Musto M, Alfano G (2013) A novel rate-dependent cohesive-zone model combining damage and visco-elasticity. Comput Struct 118:126–133

Nicolas A, Jumel J (2016) Double cantilever beam tests on a viscoelastic adhesive: effects of the loading rate. Procedia Struct Integr 2:261–276

Plausinis D, Spelt JK (1995a) Application of a new constant G load-jig to creep crack growth in adhesive joints. Int J Adhes Adhes 15(4):225–232

Plausinis D, Spelt JK (1995b) Designing for time-dependent crack growth in adhesive joints. Int J Adhes Adhes 15(3):143–154

Poblete FR, Mondal K, Ma Y, Dickey MD, Genzer J, Zhu Y (2022) Direct measurement of rate-dependent mode I and mode II traction-separation laws for cohesive zone modeling of laminated glass. Compos Struct 279:114759

Schrader P, Schmandt C, Marzi S (2022) Mode I creep fracture of rubber-like adhesive joints at constant crack driving force. Int J Adhes Adhes 113:103079

Škec L, Alafno G (2022) Experimental and numerical study of rate-dependent mode-I failure of a structural adhesive. J Adhes. https://doi.org/10.1080/00218464.2022.2106132

Xia K, Chalivendra VB, Rosakis AJ (2006) Observing ideal "self-similar" crack growth in experiments. Eng Fract Mech 73:2748–2755

Yu M, Liu B, Sun J, Feng W, Wang Q (2020) Study on improved nonlinear viscoelastic–plastic creep model based on the Nishihara Model. Geotech Geol Eng 38:1–12